Independent Observables in DVCS

Pierre Bertin, Charles E. Hyde-Wright
(Dated: 11 August 2005)

I. INTRODUCTION

Belitsky Müller and Kirchner[1] give a complete description of the kinematic dependence of the $ep \to ep\gamma$ cross section in terms of the Generalized Parton Distributions (GPD). In this note, we summarize the beam helicity (λ) dependent cross sections for unpolarized targets. We identify the independent structures that can be extracted from an analysis of the ϕ dependence of the cross section. The equation numbers in this note match the equations of [1].

The 6-fold differential cross section has the form:

$$\frac{d^6\sigma}{dQ^2 dx_{\rm Bj} d\phi_e dt dM_X^2 d\phi_{\gamma\gamma}} = \frac{\alpha^3 x_{\rm Bj}}{16\pi^2\sqrt{1+4x_{\rm Bj}^2M^2/Q^2}}\left|\frac{\mathcal{T}}{e^3}\right|^2 \otimes \frac{d\mathcal{R}}{dM_X^2}. \tag{22}$$

$d\mathcal{R}$ represents the real and virtual radiative corrections. In Eq. 22 we have integrated over φ, the azimuthal angle between the outgoing photon-proton scattering plane and the target polarization direction, and we have introduced the differential with respect to the azimuthal angle ϕ_e of the electron scattering plane.

The scattering amplitude $\mathcal{T}$ is a superposition of the Bethe-Heitler (BH) and Deeply Virtual Compton Scattering (DVCS) amplitudes:

$$|\mathcal{T}|^2 = |\mathcal{T}_{\rm BH}|^2 + |\mathcal{T}_{\rm DVCS}|^2 + \mathcal{I} \tag{23}$$

$$\mathcal{I} = \mathcal{T}^*_{\rm DVCS}\mathcal{T}_{\rm BH} + \mathcal{T}_{\rm DVCS}\mathcal{T}^*_{\rm BH} \tag{24}$$

II. AZIMUTHAL HARMONIC STRUCTURE OF THE CROSS SECTION

We propose to exploit the structure of the cross section as a function of $\phi_{\gamma\gamma}$ in order to extract a set of indepedent observables. This extraction can be done as a system of linear equations.

The individual contributions to the cross section have the form:

$$|\mathcal{T}_{\rm BH}|^2 = \frac{e^6}{x_{\rm Bj}^2 y^2[1+4x_{\rm Bj}^2M^2/Q^2]^2\Delta^2\mathcal{P}_1(\phi_{\gamma\gamma})\mathcal{P}_2(\phi_{\gamma\gamma})} \left\{c_0^{\rm BH} + \sum_{n=1}^{2} c_n^{\rm BH}\cos(n\phi_{\gamma\gamma})\right\}, \tag{25}$$

$$|\mathcal{T}_{\rm DVCS}|^2 = \frac{e^6}{y^2Q^2}\left\{c_0^{\rm DVCS} + \sum_{n=1}^{2}\left[c_n^{\rm DVCS}\cos(n\phi_{\gamma\gamma}) + s_n^{\rm DVCS}\sin(n\phi_{\gamma\gamma})\right]\right\} \tag{26}$$

$$\mathcal{I} = \frac{\pm e^6}{x_{\rm Bj}y^3\Delta^2\mathcal{P}_1(\phi_{\gamma\gamma})\mathcal{P}_2(\phi_{\gamma\gamma})} \left\{c_0^{\mathcal{I}} + \sum_{n=1}^{3}\left[c_n^{\mathcal{I}}\cos(n\phi_{\gamma\gamma}) + s_n^{\mathcal{I}}\sin(n\phi_{\gamma\gamma})\right]\right\} \tag{27}$$

Notice in the following formulae, that all $\sin(n\phi)$ terms depend on the electron helicity, and $s_3^{\mathcal{I}} = 0$. The $\phi_{\gamma\gamma}$ dependence of the cross section arises from both the fourier structure of Eq'ns 25–27, (from the virtual photon polarization) and the lepton BH Propagators:

$$\begin{aligned} Q^2\mathcal{P}_1 &= (k-q_2)^2 = Q^2 + 2k\cdot\Delta > 0, \\ Q^2\mathcal{P}_2 &= (k-\Delta)^2 = -2k\cdot\Delta + \Delta^2 < 0. \end{aligned} \tag{28}$$

The pure Bethe-Heitler cross section term $|\mathcal{T}_{\rm BH}|^2$ depends only on bilinear combinations of the ordinary elastic form factors $F_1(\Delta^2)$, $F_2(\Delta^2)$. In our analysis, we propose to set all such terms to a fixed parameterization of the experimental form factors, but to apply a single free global normalization to $|\mathcal{T}_{\rm BH}|^2$.

The harmonic coefficients of the DVCS^2 term have the form:

$$c_0^{\rm DVCS} = 2(2-2y+y^2)\mathcal{C}_{\rm unp}^{\rm DVCS}(\mathcal{F},\mathcal{F}^*) \tag{43}$$

$$\left\{\begin{array}{c} c_1^{\rm DVCS} \\ s_1^{\rm DVCS}\end{array}\right\} = \frac{8K}{2-x_{\rm Bj}}\left\{\begin{array}{c} 2-y \\ -\lambda y\end{array}\right\}\left\{\begin{array}{c}\Re\\ \Im\end{array}\right\}\mathcal{C}_{\rm unp}^{\rm DVCS}(\mathcal{F}^{\rm eff},\mathcal{F}^*), \tag{44}$$

$$c_2^{\rm DVCS} = -\frac{4Q^2K^2}{M^2(2-x_{\rm Bj})}\Re\mathcal{C}_{\rm T,unp}^{\rm DVCS}(\mathcal{F}_T,\mathcal{F}^*) \tag{45}$$

$$s_2^{\rm DVCS} = 0.$$

For an unpolarized target, the Interference observables are (in the rest we suppress the label *unp* for un-polarized target observables):

$$c_0^{\mathcal{I}} = -8(2-y)\Re\left\{\frac{(2-y)^2}{1-y}K^2\mathcal{C}^{\mathcal{I}}(\mathcal{F}) + \frac{\Delta^2}{Q^2}(1-y)(2-x_{\rm Bj})\left(\mathcal{C}^{\mathcal{I}}+\Delta\mathcal{C}^{\mathcal{I}}\right)(\mathcal{F})\right\} \tag{53}$$

$$\left\{\begin{array}{c} c_1^{\mathcal{I}} \\ s_1^{\mathcal{I}}\end{array}\right\} = 8K\left\{\begin{array}{c} -(2-2y+y^2) \\ \lambda y(2-y)\end{array}\right\}\left\{\begin{array}{c}\Re\\ \Im\end{array}\right\}\mathcal{C}^{\mathcal{I}}(\mathcal{F}) \tag{54}$$

$$\left\{\begin{array}{c} c_2^{\mathcal{I}} \\ s_2^{\mathcal{I}}\end{array}\right\} = \frac{16K}{2-x_{\rm Bj}}\left\{\begin{array}{c} -(2-y) \\ \lambda y\end{array}\right\}\left\{\begin{array}{c}\Re\\ \Im\end{array}\right\}\mathcal{C}^{\mathcal{I}}(\mathcal{F}^{\rm eff}) \tag{55}$$

$$c_3^{\mathcal{I}} = -\frac{8Q^2K^3}{M^2(2-x_{\rm Bj})^2}\Re\left[{\mathcal{C}^{\mathcal{I}}}_T(\mathcal{F}_T)\right] \tag{56}$$

$$s_3^{\mathcal{I}} = 0$$

Table I summarizes the independent angular harmonics. The precise definitions are given in terms of the GPDs in Eq. 66–83 of Belitsky[1]. They have the basic form:

- $\mathcal{C}^{DVCS}(\mathcal{F},\mathcal{F}^*)$ is a (real) bi-linear combination of the Twist-2 quark GPDs $\mathcal{F}=\{\mathcal{H},\mathcal{E},\tilde{\mathcal{H}},\tilde{\mathcal{E}}\}$
- $\mathcal{C}^{DVCS}(\mathcal{F}^{\rm eff},\mathcal{F}^*)$ is the same bi-linear combination, but it is complex because the $\mathcal{F}^{\rm eff}$ include effective Twist-3 GPDs (Wanzura-Wilxec)
- $\mathcal{C}_T^{\rm DVCS}(\mathcal{F}_T,\mathcal{F}^*)$ is the interference of the Twist-2 Gluon Transversity GPDs $\mathcal{F}_T$ with the ordinary GPDs $\mathcal{F}$.
- $\mathcal{C}^{\mathcal{I}}(\mathcal{F})$ is the interference of the BH amplitude with the Twist-2 quark GPDs.
- $\Delta\mathcal{C}^{\mathcal{I}}(\mathcal{F})$ also depends on the twist-2 quark GPDs, but is kinematically suppressed by a factor $x_{\rm Bj}$. *This term arises from the corrections to restore EM Gauge invariance at the twist-2 level??*
- $\mathcal{C}^{\mathcal{I}}(\mathcal{F}^{\rm eff})$ has the same form as $\mathcal{C}^{\mathcal{I}}(\mathcal{F})$, but depends upon the WW effective Twist-3 GPDs ($\mathcal{F}^{\rm eff}$).
- $\mathcal{C}_T^{\mathcal{I}}(\mathcal{F}_T)$ is the interference of the four Twist-2 Gluon Transversity GPDs $\mathcal{F}_T$ with the BH amplitude.

III. EXTRACTION OF OBSERVABLES

We develop a general notation to explain the proceedures for extracting the observables of Table I from the data. Fig. 1 illustrates our notation. Let

$$\mathbf{x}_v = \{k, x_{\rm Bj}, Q^2, \Delta^2, \phi_e, \phi_{\gamma\gamma}, z\}_v \tag{III-1}$$

represent the kinematic variables at the event vertex (in the simulation). The incident electron energy k is included, in order to treat the radiative tail. Let

$$\mathbf{x}_e = \{x_{\rm Bj}, Q^2, \Delta^2, \phi_e, \phi_{\gamma\gamma}\}_e \tag{III-2}$$

represent the event variables, as reconstructed by the detector. In the Monte-Carlo simulation, we define the mapping

$$K(\mathbf{x}_e|\mathbf{x}_v) \tag{III-3}$$

	Unknown	Type	ϕ dependance	Eq.
BH^2	normalisation constant	Elastic	$\mathcal{P}_1^{-1}\mathcal{P}_2^{-1}\,(c_o$	35
		Form	$+c_1\cdot\cos(\phi)$	36
		Factors^2	$+c_2\cdot\cos 2\phi)$	37
$DVCS^2$	$C_{unp}^{DVCS}(\mathcal{F},\mathcal{F}^*)$	twist-2	c^t	43
	$\Re[C_{unp}^{DVCS}(\mathcal{F}^{eff},\mathcal{F}^*)]$	twist-3	$\cos\phi$	44
	$\Im[C_{unp}^{DVCS}(\mathcal{F}^{eff},\mathcal{F}^*)]$	twist-3	$\sin\phi$	44
	$\Re[C_{unp}^{DVCS}(\mathcal{F}_T,\mathcal{F}^*)]$	twist-3	$\cos 2\phi$	45
$BH\cdot$ $DVCS$	$\Re[C_{unp}^{I}(\mathcal{F})]$	twist-2	$\mathcal{P}_1^{-1}\mathcal{P}_2^{-1}$	53
			$\mathcal{P}_1^{-1}\mathcal{P}_2^{-1}\cos\phi$	54
	$\Re[\Delta C_{unp}^{I}(\mathcal{F})]$	twist-2++	$\frac{1}{\mathcal{P}_1\mathcal{P}_2}$	53
	$\Im[C_{unp}^{I}(\mathcal{F})]$	twist-2	$\frac{\lambda}{\mathcal{P}_1\mathcal{P}_2}\sin\phi$	54
	$\Re[C_{unp}^{I}(\mathcal{F}^{eff})]$	twist-3	$\frac{1}{\mathcal{P}_1\mathcal{P}_2}cos2\phi$	55
	$\Im[C_{unp}^{I}(\mathcal{F}^{eff})]$	twist-3	$\frac{\lambda}{\mathcal{P}_1\mathcal{P}_2}\sin 2\phi$	55
	$\Re[C_{T,unp}^{I}(\mathcal{F}_T)]$	twist-2 gluon	$\frac{1}{\mathcal{P}_1\mathcal{P}_2}\cos 3\phi$	56

TABLE I: The 11 independant unknown quantities (including one normalisation coefficient) that can be extracted from the data. The forth column gives the formal ϕ dependence of each term. The last column is the the equation label of the A.V. Belitsky-D. Muller paper. Each of the 11 unknowns can be binned in ξ, $\Delta^2 = t$, and Q^2.

as the conditional probability distribution to observe an event at the kinematic point $\mathbf{x}_e$, starting from vertex point $\mathbf{x}_v$. The experimental acceptances, efficiencies, and resolution are included in K. Let $d\mathcal{R}$ define the radiative effects generating a flux of electrons, differential in k. The binning vector

$$\mathbf{i}_e \;=\; \{i_\xi, i_{Q^2}, i_{\Delta^2}\}_e \tag{III-4}$$

labels a set of bins in the corresponding event kinematics, after integration over ϕ_e and $\phi_{\gamma\gamma}$. The binning vector

$$\mathbf{j}_v \;=\; \{j_\xi, j_{Q^2}, j_{\Delta^2}\}_e \tag{III-5}$$

labels a similar set of bins in the vertex variables. The vector $\mathbf{X_j} = X_{\mathbf{j}}^{(\Lambda)}$ defines the set of observables $\mathcal{C}$, $\Delta\mathcal{C}\ldots$ of Table I averaged over the bins $\mathbf{j}_v$ of Eq. III-5. The index Λ identifies the observable. The functions

$$F^{(\Lambda)}(\mathbf{x}_v) \tag{III-6}$$

are the kinematic factors defined schematically in column 4 of Table I and explicitly in Eqs. 35–65 of [1], including the prefactors of Eqs. 22,25–27.

We define a bin mapping function:

$$\mathbf{K}_{\mathbf{i}_e,\mathbf{j}_v} = K^{(\Lambda)}_{\mathbf{i}_e,\mathbf{j}_v} \;=\; \int_{\mathbf{x}_e\in \mathrm{Bin}(\mathbf{i}_e)}\int_{\mathbf{x}_v\in \mathrm{Bin}(\mathbf{j}_v)} d\mathcal{R}K(\mathbf{x}_e|\mathbf{x}_v)F^{(\Lambda)}(\mathbf{x}_v) \tag{III-7}$$

The integrated experimental luminosity is $\int \mathcal{L}dt$. For a given set of values $\mathbf{X}_{\mathbf{j}_v}$, the expected yield (number of counts per bin) is:

$$Y^{MC}(\mathbf{i}_e) \;=\; \left[\int \mathcal{L}dt\right]\sum_{\mathbf{j}_v,\Lambda} K^{(\Lambda)}_{\mathbf{i}_e,\mathbf{j}_v}X^{(\Lambda)}_{\mathbf{j}_v} \tag{III-8}$$

We can now construct a chi-square, which can be minimized to extract the $\mathbf{X_j}$:

$$\chi^2 \;=\; \sum_{\mathbf{i}_e}\frac{\left[Y^{\mathrm{Exp}}(\mathbf{i}_e) - Y^{MC}(\mathbf{i}_e)\right]^2}{\left[\sigma^{\mathrm{Exp}}(\mathbf{i}_e)\right]^2}, \tag{III-9}$$

where $\sigma^{\mathrm{Exp}}(\mathbf{i}_e)$ are the experimental error-bars in each bin.

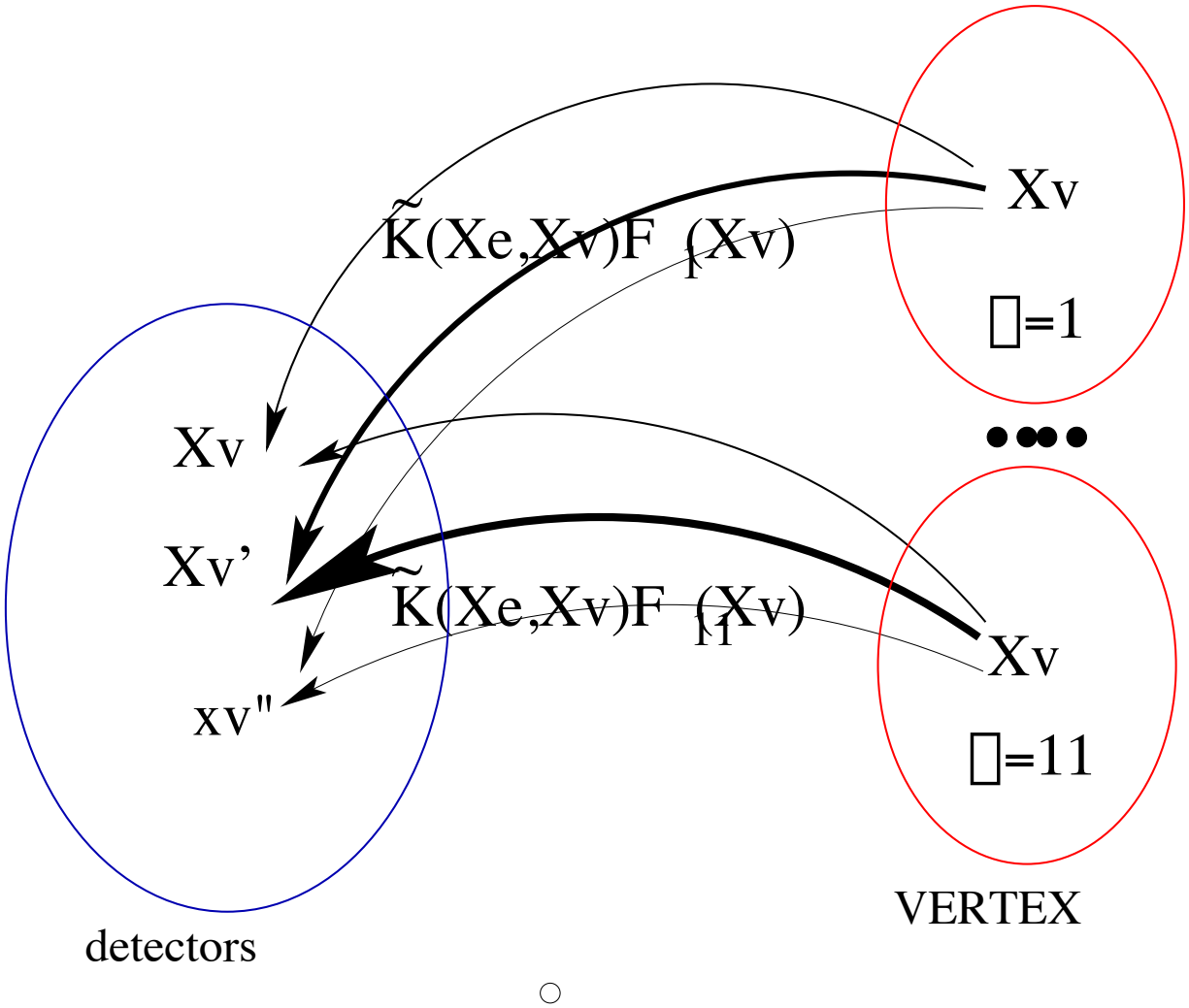

FIG. 1: Schematic representation of the measurement and simulation process. A given event is defined by the kinematic vector $\mathbf{X_v}$ at the vertex. The physics vertex kinematic space is illustrated by the red circles at right. As a result of multiple scattering, straggling, bremsstrahlung, optical aberations in the spectrometer, *etc.*, the event is reconstructed with kinematics $\mathbf{X_e}$. The reconstructed event space is illustrated by the blue circle at left. Notice that a given physics event $\mathbf{X_v}$ can end up at multiple locations $\mathbf{X'_e}$, $\mathbf{X''_e}$ in the event space. This is indicated by the multiple arrows, labelled by the conditional probability distribution K. The event space at right is replicated 11 times to represent the eleven independent physics observables defined in Table I. In the simulation, for each projection $\mathbf{X_v} \mapsto \mathbf{X_e}$, we apply the eleven kinematic weight factors $F^{(\Lambda)}$ to the probability distribution $K(\mathbf{X_e}|\mathbf{X_v})$.

Notice that the vector $X^{(\Lambda)}_{\mathbf{j}_v}$ is an outer product with respect to its two indices $\mathbf{j}_v$ and Λ. The coefficients $\overline{\mathbf{X}}_{\mathbf{j}_v}$ are defined as the values of $\mathbf{X}_{\mathbf{j}_v}$ that minimize χ^2:

$$0 = -\frac{1}{2}\left.\frac{\partial\chi^2}{\partial X^{(\Lambda)}_{\mathbf{j}_v}}\right|_{\overline{\mathbf{X}}_{\mathbf{j}_v}} \tag{III-10}$$

$$0 = \sum_{\mathbf{i}_e}\left[\int \mathcal{L}dt\right] K^{(\Lambda)}_{\mathbf{i}_e,\mathbf{j}_v}\frac{\left[\int \mathcal{L}dt\right]\sum_{\mathbf{j}'_v,\Lambda'} K^{(\Lambda')}_{\mathbf{i}_e,\mathbf{j}'_v}\overline{X}^{(\Lambda')}_{\mathbf{j}'_v} - Y^{\mathrm{Exp}}(\mathbf{i}_e)}{\left[\sigma^{\mathrm{Exp}}(\mathbf{i}_e)\right]^2} \tag{III-11}$$

$$0 = \sum_{\mathbf{j}'_v,\Lambda'} \alpha^{(\Lambda),(\Lambda')}_{\mathbf{j}_v,\mathbf{j}'_v}\overline{X}^{(\Lambda')}_{\mathbf{j}'_v} - \beta^{(\Lambda)}_{\mathbf{j}_v} \quad \forall\, \mathbf{j}_v,\, \Lambda. \tag{III-12}$$

The linear system is defined by:

$$\alpha^{(\Lambda),(\Lambda')}_{\mathbf{j}_v,\mathbf{j}'_v} \;=\; \sum_{\mathbf{i}_e} \left[\int \mathcal{L}dt\right]^2 K^{(\Lambda)}_{\mathbf{i}_e,\mathbf{j}_v} K^{(\Lambda')}_{\mathbf{i}_e,\mathbf{j}'_v} \Big/ \left[\sigma^{\rm Exp}(\mathbf{i}_e)\right]^2 \tag{III-13}$$

$$\beta^{(\Lambda)}_{\mathbf{j}_v} \;=\; \sum_{\mathbf{i}_e} Y^{\rm Exp}(\mathbf{i}_e) \left[\int \mathcal{L}dt\right] K^{(\Lambda)}_{\mathbf{i}_e,\mathbf{j}_v} \Big/ \left[\sigma^{\rm Exp}(\mathbf{i}_e)\right]^2 \tag{III-14}$$

The fit parameters are:

$$\overline{X}^{(\Lambda)}_{\mathbf{j}_v} \;=\; \sum_{\mathbf{j}'_v,\Lambda'} \left[\alpha^{-1}\right]^{(\Lambda),(\Lambda')}_{\mathbf{j}_v,\mathbf{j}'_v} \beta^{(\Lambda')}_{\mathbf{j}'_v}. \tag{III-15}$$

The covariance matrix of the fitted parameters is:

$$V^{(\Lambda,\Lambda')}_{\mathbf{j}_v,\mathbf{j}'_v} \;=\; \left[\alpha^{-1}\right]^{(\Lambda),(\Lambda')}_{\mathbf{j}_v,\mathbf{j}'_v}. \tag{III-16}$$

IV. MODEL DEPENDENT IMPROVEMENT TO THE FIT

There is a systematic error in the proceedure defined above. The observables $\mathbf{X}_{\mathbf{j}_v}$ are taken at the center of the kinematic bin $\mathbf{j}_v$. However, if we maximize our statistics, and use only one bin $\Delta\xi = 0.5$, then the observables can vary by as much as a factor of two within the bin. We can resolve this problem (or at least provide an estimate of the resulting uncertainty) by incorporating a model of the observables $\mathbf{X}_{\mathbf{j}_v}$ **into our definitions of the kinematic functions** $F^{(\Lambda)}(\mathbf{x}_v)$. To wit:

$$F^{(\Lambda)\,\rm Model}(\mathbf{x}_v) \;=\; F^{(\Lambda)}(\mathbf{x}_v) X^{(\Lambda)\,\rm Model}(\mathbf{x}_v) \Big/ X^{(\Lambda)\,\rm Model}_{\mathbf{j}_v(\mathbf{x}_v)}, \tag{IV-17}$$

where $X^{(\Lambda)\,\rm Model}(\mathbf{x}_v)$ are the values of the observables evaluated in the model at the kinematic point $\mathbf{x}_v$ and $X^{(\Lambda)\,\rm Model}_{\mathbf{j}_v(\mathbf{x}_v)}$ are the values of the observables evaluated in the model at the center of the bin $\mathbf{j}_v$ corresponding to the kinematic point $\mathbf{x}_v$. In this way the fitted values $\overline{X}^{(\Lambda)}_{\mathbf{j}_v}$ will be the experimental values at the center of the bin, evaluated with the full model dependence inside the bin.

V. MONTE CARLO INTEGRATION

The integrated bin mapping function $K^{(\Lambda)}_{\mathbf{i}_e,\mathbf{j}_v}$ of Eq. III-7 is calculated by Monte Carlo simulation. In general, a monte carlo integration is defined as follows [2]:

$$\int f(\mathbf{x})\rho(\mathbf{x})d^m\mathbf{x} \;\rightarrow\; V\left\langle f\right\rangle \pm \frac{V}{\sqrt{N}}\sqrt{\left\langle f^2\right\rangle - \left\langle f\right\rangle^2}$$

$$\left\langle f\right\rangle \;=\; \frac{1}{N}\sum_{i=1}^{N} f(\mathbf{x}_i)$$

$$\left\langle f^2\right\rangle \;=\; \frac{1}{N}\sum_{i=1}^{N} f^2(\mathbf{x}_i) \tag{V-18}$$

The random events $\mathbf{x}_i$ are chosen with probability distribution $\rho(\mathbf{x}_i)$ in the volume V.

In our case the monte carlo integration is complicated by the radiative effects (external and internal). The vertex variables $x_{\rm Bj}$, Q^2, ϕ_e, t, $\phi_{\gamma\gamma}$, and z are chosen with uniform distributions. All the variables except t are chosen in a fixed interval. Because of the kinematic bounds, t is chosen in the interval:

$$t \;\in\; \left[t_{\rm Max}, t_{\rm Min}(x,Q^2)\right] \tag{V-19}$$

In principle, $t_{\rm Max}$ also depends on the kinematics, but we chose a small enough absolute value that is does not matter Thus each event receives a phase space weight:

$$\Delta\Gamma/N \;=\; \Delta z \Delta x_{\rm Bj} \Delta Q^2 \Delta\phi_e 2\pi \Delta t(x_{\rm Bj}, Q^2)/N \tag{V-20}$$

A. Radiative Lineshape

We generate the radiative lineshape with its intrinsic distribution, and not with a uniform event generator. The vertex position defines the target radiation thickness $t_i(z)$ in the initial state. The external radiation in the initial state is obtained by defining $\Delta k_i^{\rm Ext} = k_0 R_{\rm Ext}^{1/(bt_i)}$[3], where $b \approx 4/3$ is the Mo & Tsai parameter and $R_{\rm Ext}$ is a uniform random variable on the interval $[0,1]$. This generates an external radiation distribution

$$I_{\rm Ext}(k_0, \Delta k_i^{\rm Ext}, t_i) \;=\; \frac{1}{k_0 b t_i}\left(\frac{\Delta k_i^{\rm Ext}}{k_0}\right)^{bt_i - 1}. \tag{V-21}$$

The internal radiation at the vertex is handled with the same algorithm. The radiation is treated in the peaking approximation, and is split between the initial and final states. The internal radiation along the incident beam direction is (R iInts another uniform deviate) [4]

$$\Delta k_i^{\rm Int} \;=\; (k_0 - \Delta k_i^{\rm Ext}) R_{\rm Int}^{2/\delta} \tag{V-22}$$

$$I_{\rm Int}(k_0 - \Delta k_i^{\rm Ext}, \Delta k_i^{\rm Int}) \;=\; \frac{2}{\delta}\frac{1}{\Delta k_i^{\rm Int}}\left(\frac{\Delta k_i^{\rm Int}}{k_0 - \Delta k_i^{\rm Ext}}\right)^{\delta/2} \tag{V-23}$$

$$\delta \;=\; \frac{\alpha}{\pi}\ln\left[\frac{Q^2}{m_e^2}\right] \tag{V-24}$$

The incident electron energy at the vertex is

$$k_v \;=\; k_0 - \Delta k_i^{\rm Ext} - \Delta k_i^{\rm Int} \tag{V-25}$$

The scattered electron energy at the vertex is

$$k'_v \;=\; k - \nu(x_{\rm Bj}, Q^2) = k - Q^2/[2M(x_{\rm Bj}]. \tag{V-26}$$

The electron scattering angle at the vertex is defined by:

$$\cos\theta_v \;=\; Q^2/(2k_v k'_v). \tag{V-27}$$

The post radiation (internal and external) are treated in the same way. The internal post radiation (along the direction θ_v of k'_v) is [5]:

$$\Delta k_f^{\rm Int} \;=\; k'_v R_{\rm Int,f}^{2/\delta} \tag{V-28}$$

$$I_{\rm Int}(k'_v, \Delta k_f^{\rm Int}) \;=\; \frac{2}{\delta}\frac{1}{\Delta k_f^{\rm Int}}\left(\frac{\Delta k_f^{\rm Int}}{k'_v}\right)^{\delta/2} \tag{V-29}$$

From the scattered trajectory, the final thickness in radiation lengths of the exit electron trajectory is $t_f(z_v, \theta_v, \phi_e)$. The external radiation distribution is:

$$\Delta k_f^{\rm Ext} \;=\; (k'_v - \Delta k_f^{\rm Int}) R_{\rm Ext,f}^{1/(bt_f)} \tag{V-30}$$

$$I_{\rm Ext}(k'_v - \Delta k_f^{\rm Int}, \Delta k_f^{\rm Ext}, t_f) \;=\; \frac{1}{(k'_v - \Delta k_f^{\rm Int}) b t_i}\left(\frac{\Delta k_f^{\rm Ext}}{(k'_v - \Delta k_f^{\rm Int})}\right)^{bt_f - 1}. \tag{V-31}$$

The final energy of the electron, leaving the target is

$$k' \;=\; k'_v - \Delta k_f^{\rm Int} - \Delta k_f^{\rm Ext} \tag{V-32}$$

B. Monte Carlo Variables

The complete set of uniform random variables at the vertex are:

$$\{z,\, x_{\rm Bj},\, Q^2,\, R_i^{\rm Ext},\, R_i^{\rm Int},\, \phi_e,\, R_f^{\rm Int},\, R_f^{\rm Ext},\, \Delta^2 = t,\, \phi_{\gamma\gamma}\} \tag{V-33}$$

Notice that the variables must be generated in the order listed.

Because the vertex position is a random variable, the effective target length is determined by the simulation. It is incorrect to normalize the simulation by the integrated luminosity $\int \mathcal{L} dt$. Instead, the simulated yield must be normalized by

$$\int \frac{d\mathcal{L}}{dz} dt \;=\; \frac{Q}{e} \rho_{H_2}, \tag{V-34}$$

where Q is the integrated beam charge and ρ is the target density in nuclei/cm^2.

VI. INCLUDING THE MONTE-CARLO ERROR BARS

The statistical analysis presented above includes only the experimental uncertainties $\sigma^{\rm Exp}(\mathbf{i}_e)$ in each kinematic bin. However, the simulation of the mapping function $K^{(\Lambda)}_{\mathbf{i}_e,\mathbf{j}_v}$ also has a monte-carlo statistical uncertainty. How can we include these simulation uncertainties into the covariance matrix of the fitted observables $\mathbf{X}_{\mathbf{j}_v}$?

Notice that the only rôle of the experimental error bars is to define the bin by bin weight of χ^2 in Eq. III-9. We define a monte carlo uncertainty:

$$\sigma^{MC}(\mathbf{i}_e) \;=\; \text{Monte Carlo error on } \; Y^{MC}(\mathbf{i}_e). \tag{VI-35}$$

The monte carlo and experimental error bars are independent. Thus in the definitions of χ^2, α, and β (Eq. III-9,III-13,III-14) we can make the substitutions:

$$\left[\sigma^{\rm Exp}(\mathbf{i}_e)\right]^2 \;\rightarrow\; \left[\sigma^{\rm Exp}(\mathbf{i}_e)\right]^2 + \left[\sigma^{MC}(\mathbf{i}_e)\right]^2 \tag{VI-36}$$

Unfortunately, this introduces a model dependence, or non-linearity, to the fit. The bin mapping matrix elements K have monte carlo statistical uncertainties δK. Therefore the uncertainties in Y^{MC} are:

$$\left[\sigma^{MC}(\mathbf{i}_e)\right]^2 \;=\; \left[\int \mathcal{L} dt\right]^2 \sum_{\Lambda} \left[\delta K^{(\Lambda)}_{\mathbf{i}_e,\mathbf{j}_v}\right]^2 \left[X^{(\Lambda),\rm Model}_{\mathbf{j}_v}\right]^2 \tag{VI-37}$$

Thus it is necessary to either include a model of $\mathbf{X}$, or to iterate on the fitted values $\overline{\mathbf{X}}$. It is also necessary to consider whether the monte carlo uncertainties $\delta K^{(\Lambda)}_{\mathbf{i}_e,\mathbf{j}_v}$ are truely statistically independent.

VII. POISSON STATISTICS

The χ^2 minimization proceedure described above is based on gaussian statistics, which is valid if the number of events per bin is large. In principle, we should use Poisson statistics, which are exact for all low count rate experiments (relative to the beam intensity). If some of the observables are predominantly determined by low statistics bins then there is a systematic error in gaussian statistics, arising from the asymmetry of the poisson distribution.

A. Gaussian Overfit of Poisson Statistics

We illustrate the problem of applying Gaussian statistics to a Poisson statistics problem. Let $N(i)$ be the set of counts per bin in an experiment. Let $y(i) = \sum_j a_j f_j(i)$ be a fitting function. Then we define the usual χ^2:

$$\chi^2 = \sum_i \frac{\left[y(i) - \sum_j a_j f_j(i)\right]^2}{\sigma(i)^2}. \tag{VII-38}$$

After minimizing χ^2, the fitted parameters and the minimized value of χ^2 are:

$$\overline{a}_j \;=\; \left[\alpha^{-1}\right]_{j,k} \beta_k \tag{VII-39}$$

$$\alpha_{j,k} \;=\; \sum_i f_j(i) f_k(i) / \sigma(i)^2 \tag{VII-40}$$

$$\beta_k = \sum_i y(i) f_k(i) / \sigma(i)^2 \tag{VII-41}$$

$$\overline{\chi}^2 = \sum_i \frac{\left[y(i) - \sum_j \overline{a}_j f_j(i)\right]^2}{\sigma(i)^2} \tag{VII-42}$$

$$= \sum_i \frac{y(i)^2}{\sigma(i)^2} - \beta_j {\alpha^{-1}}_{j,k} \beta_k \tag{VII-43}$$

We can approximate Poisson statistics by setting $\sigma(i)^2 = y(i)$. Then we find that the fit systematically underestimates the data by an amount exactly equal to $\overline{\chi}^2$:

$$\overline{\chi}^2 = \sum_i y(i) - \beta_j {\alpha^{-1}}_{j,k} \beta_k \tag{VII-44}$$

$$\beta_j(\text{Poisson}) = \sum_i f_j(i) \tag{VII-45}$$

$$\sum_i \left[y(i) - \overline{a}_j f_j(i)\right] = \sum_i \left[y(i) - f_j(i) {\alpha^{-1}}_{j,k} \beta_k\right]$$

$$= \sum_i y(i) - \beta_j {\alpha^{-1}}_{j,k} \beta_k$$

$$= \overline{\chi}^2 \tag{VII-46}$$

We expect the minimized value $\overline{\chi}^2$ to be nearly equal to the number of bins minus the number of free parameters. As long as the total number of events is much larger than $\overline{\chi}^2$, the systematic underfit is not a major problem. However, even if the statistics are high, if there are parameters that are determined mostly by low statistics kinematic regions, then the underfit can strongly bias the extracted parameters. The resulting error can be greater than the statistical uncertainty on the small paraemter.

The underfit problem can be partially resolved by setting $\sigma(i)^2 = y(i) + 1$. This has the virtue of defining a finite statistical error for bins with zero counts, and reflects the fact that for the Poisson distribution, the most probable value is approximately 1 less than the mean. A better correction is to set $\sigma(i)^2$ not equal to the data, but equal to the fit. After all, the conjecture of the fit is that the data are obtained from a parent Poisson distribution whose mean is equal to the fitted value. In the extreme cases of bins with zero counts, the fit will generally give a fraction of a count, with appropriate error bar. This method has the strong disadvantage that we no longer obtain linear minimization problem.

VIII. KINEMATIC SENSITIVITY TO PHYSICS OBSERVABLES

In Fig. 2, we plot the kinematic weight factors $F^{(\Lambda)}$ of the BH-DVCS interference terms. In each case, we compare with the full BH term $|\mathcal{T}_{BH}/e^3|^2$ (including the elastic form factors). Notice that the weight factor for the Gluon Transversity term $\Re[C^I(F_T)]$ is very small, but growing with $-t$.

In Fig. 3, we display similar plots of the kinematic weight factors $F^{(\Lambda)}$ of the DVCS^2 cross section terms.

[1] A.V. Belitsky, D. Müller, A. Kirchner, hep-ph/0112108

[2] **Numerical Recipes**, W. Press, S. Teukolsky, W. Vetterling, B Flannery, §7.6, `www.library.cornell.edu/nr/cbookcpdf.html`

[3] DVCS Analysis Code object TGenBase::ExtBrem(), `http://www.jlab.org/~munoz/gen/MY_Index.html`

[4] DVCS Analysis Code object TGenDVCS::IntRCBef()

[5] DVCS Analysis Code object TGenDVCS::IntRCAft()

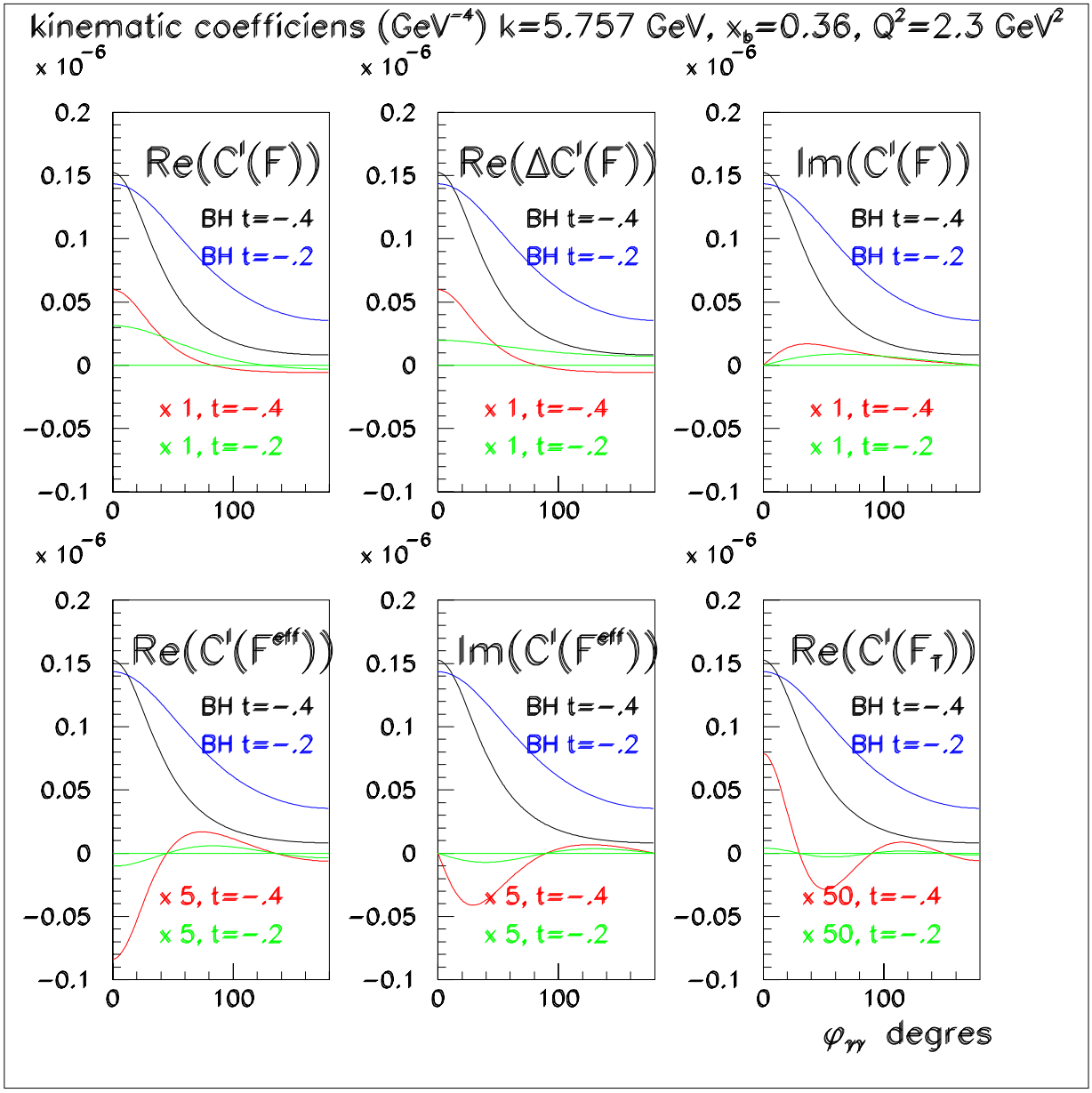

FIG. 2: Kinematic factors $F^{(\Lambda)}$, which weight the physics observables in DVCS. The blue and black curves are the complete $|\mathcal{T}_{BH}|^2$ terms, evaluated at $-t = 0.2$ and 0.4 GeV^2, respectively. The six panels display the kinematic weight factors of the BH-DVCS interference observables. The green and red curves give the kinematic weight factors $F^{(\Lambda)}$ at $-t = 0.2$ and 0.4 GeV^2, respectively. The $\Im C^I(F)$ term is the helicity dependent $\sin\phi$ term which is the focus of most of the DVCS experimental work. Notice that the interference amplitudes in the top three panels are normalized by one. In the bottom three panels, the interference amplitudes are amplified by factors of 5, 5, and 50, from left to right, to enhance their visibility on the plots.

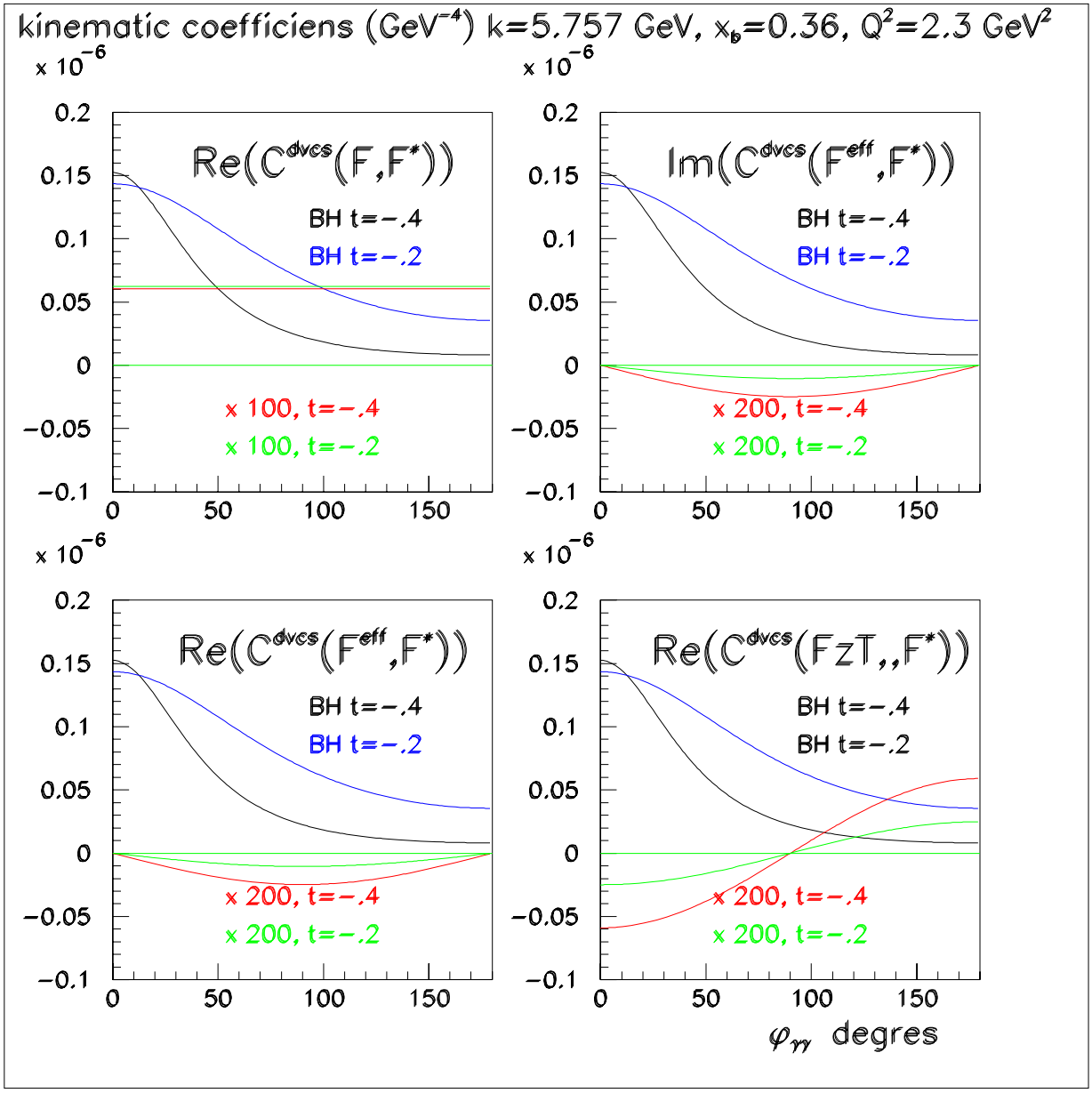

FIG. 3: Kinematic factors $F^{(\Lambda)}$, which weight the physics observables in DVCS (same conventions as Fig. 2). The blue and black curves are the complete $|\mathcal{T}_{BH}|^2$ terms, evaluated at $-t = 0.2$ and 0.4 GeV^2, respectively. The four panels display the kinematic weight factors of the $|\mathcal{T}_{DVCS}|^2$ terms. Notice the normalization factors applied to the DVCS terms.